Metal-Organic Frameworks and Porous Coordination Polymers: Properties and Applications†

[a]Department of Chemistry, Seoul National University, Seoul 151-747
[b]Department of Chemistry, Hanyang University, Seoul 133-791, Republic of Korea
Myunghyun Paik Suh*[a,b]

Received March 19, 2015; E-mail: mpsuh@snu.ac.kr

In this review, properties and applications of metal-organic frameworks (MOFs) and porous coordination polymers (PCPs) are described. Many MOFs and PCPs are highly flexible and responsive to external stimuli. Sometimes they transform their structures to others by maintaining the single crystallinity. For decades, MOFs and PCPs have been regarded as a class of the promising materials for hydrogen storage and carbon dioxide capture applications since they adsorb large amounts of gases at low temperatures. However, their gas uptake capacities decrease dramatically at ambient temperature compared to those at low temperatures because they physic-sorb gases by weak interaction energies. Therefore, to enhance gas storage and separation abilities of MOFs and PCPs at ambient temperature, we have modified their pore spaces. In this review, some characteristic properties of MOFs and PCPs will be introduced, and various strategies for modifying the pore spaces of PCPs and MOFs for hydrogen storage and carbon dioxide capture will be presented.

†Based on parts of the lecture given at the 64th Conference of the Japan Society of Coordination Chemistry, held in Tokyo from September 19-21, 2014, on the occasion of the International Award 2014 of the Japan Society of Coordination Chemistry.

1. Introduction

Metal-organic frameworks (MOFs) and porous coordination polymers (PCPs) generally have defined structures, permanent porosity, and high specific surface areas. They are synthesized from metal and organic building blocks by solvothermal reactions or self-assembly. MOFs and PCPs are considered to be a class of the most promising materials for hydrogen storage and for gas separation such as carbon dioxide capture from the flue gas or natural gas. However, gas adsorption on the pore surface of MOFs and PCPs is physisorption, and the interaction energy between the adsorbents and gas is too weak. Therefore, even though large amount of gases can be stored in the materials at a low temperature, the storage capacity falls down to very low values at ambient temperature. To enhance hydrogen gas storage in MOFs and PCPs, we have modified their pore spaces by various methods such as generating accessible metal sites, fabricating metal nanoparticles (NPs), including proper organic guests, and incorporating specific metal ion binding sites in the ligand. The generation of accessible metal sites is based on "Kubas" interactions of hydrogen molecules with the metal ions. The production of metal nanoparticles in PCPs, without using extra reducing agent and NP-stabilizing agents just at room temperature, is based on the redox chemistry between the redox-active components of the MOFs or PCPs and the metal ions. To capture CO_2 selectively from the industry flue gas that contains not only CO_2 but also other gases, we have developed smart 3-dimensional (3D) PCPs with very small pores, which are highly flexible. Since CO_2 molecule has much higher polarizability and quadrupole moment than other gases, it would interact much more strongly with the flexible PCPs with very small pores and open up the windows while other gases cannot. We have also created various strategies such as post-synthetic modification of pore space with highly flexible carboxyl pendants, impregnation of metal ions in the pores of a MOF, and inclusion of branched polyethylenimine units in the pores of porous organic polymer. These induce stronger interactions with the CO_2 molecules, and enhance the gas uptake capacities and the selectivity of CO_2 adsorption

Corresponding Author: Myunghyun Paik Suh
Address: Department of Chemistry, Hanyang University, 222 Wangsimni-ro, Seongdong-gu, Seoul 133-791, Republic of Korea.
Tel: +82 02-2220-0922 Fax: +82 02-887-7767
Keywords: metal-organic frameworks, porous coordination polymers, hydrogen storage, carbon dioxide capture, metal nanoparticles, crown ether, isosteric heat, selectivity

from the mixture gas. This review is based on the award lecture, and presents the properties of MOFs and PCPs and various strategies for modifying their pore spaces for hydrogen storage and carbon dioxide capture applications.

2. Synthetic methods of MOFs and PCPs

2.1. Solvothermal reactions

Metal-organic frameworks (MOFs) and porous coordination polymers (PCPs) can be synthesized from metal and organic building blocks by the solvothermal reactions or self-assembly at room temperature.[1,2] In particular, when the metal salts are heated with carboxylic acid, metal forms metal cluster units that have specific geometries, so called secondary building units (SBUs).[1] By the combination of SBUs and ligands, which have specific geometries, various types of 3D MOFs can be constructed as described in Fig. 1. In these MOFs and PCPs, SBUs generally are located at the nodes of the frameworks and the ligands at the struts.

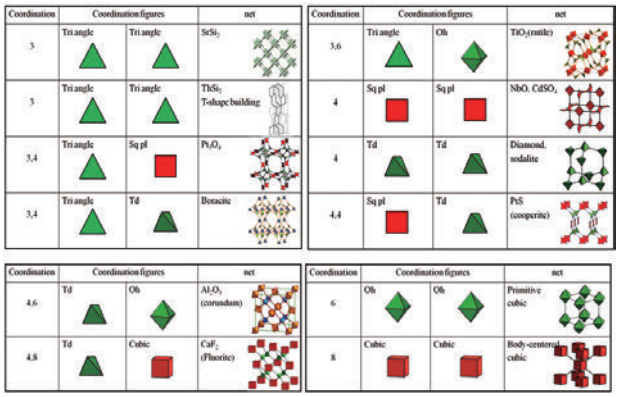

Fig. 1 Various framework structures constructed from the combination of metal clusters and organic ligands.

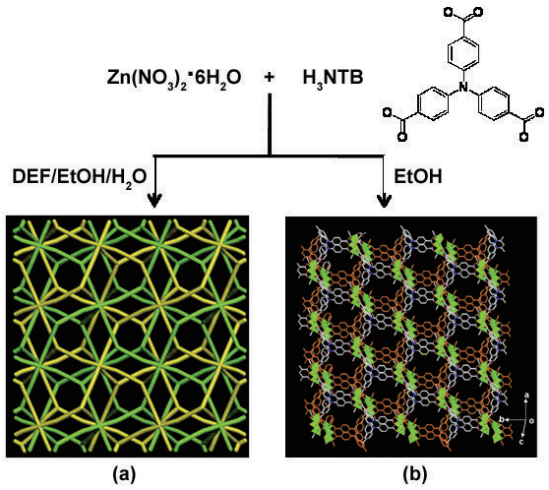

Fig. 2 Two different frameworks formed from Zn(II) and H_3NTB in the different solvent systems. (a) $[Zn_4O(NTB)_2]\cdot 3DEF\cdot EtOH$ having doubly interpenetrated PdF_2 structure.[3] (b) $[Zn_3(NTB)_2(EtOH)_2]\cdot 4EtOH$.[4]

In the solvothermal synthesis of MOFs, reaction conditions such as solvent system and reaction temperature determine the resulting framework structures. For example, when $Zn(NO_3)_2 6H_2O$ and 4,4',4"-nitrilotrisbenzoic acid (H_3NTB) are heated in the mixed solvent system of DEF/EtOH/H_2O and EtOH, respectively, different MOFs, $[Zn_4O(NTB)_2]_n\cdot 3n$DEF$\cdot n$EtOH and $[Zn_3(NTB)_2(EtOH)_2]_n\cdot 4n$EtOH, are resulted (Fig. 2).[3,4]

In addition, the presence or absence of small amount of acid in the solvent system also affects the product. For example, two different 3D MOFs, $[Zn_4O(NTN)_2]\cdot 10DMA\cdot 7H_2O$ (**SNU-150**) and $[Zn_5(NTN)_4(DEF)_2][NH_2(C_2H_5)_2]_2\cdot 8DEF\cdot 6H_2O$ (**SNU-151**), were synthesized from the same metal and organic building blocks but in the different solvent systems, particularly in the absence and the presence of small amount of acid (Fig. 3).[5] **SNU-150** is a doubly interpenetrated neutral framework while **SNU-151** is a non-interpenetrated anionic framework including diethylammonium cations in the pores. Although charged MOF **SNU-151** has smaller surface area (BET, 1563 $m^2 g^{-1}$) than the neutral MOF **SNU-150** (BET, 1852 $m^2 g^{-1}$), the former exhibits superior gas storage and gas separation abilities than the latter.

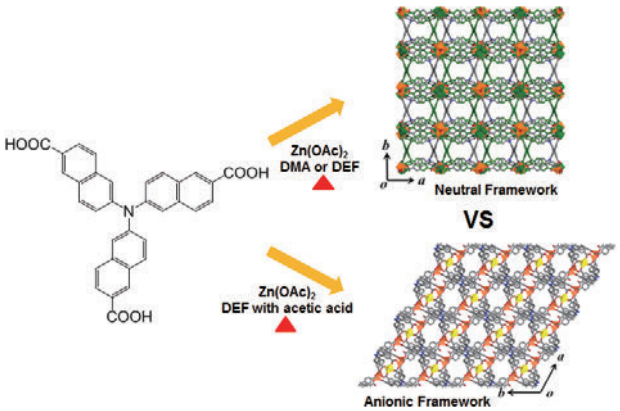

Fig.3 Preparation of neutral framework **(SNU-150)** and charged framework **(SNU-151)** in the presence and absence of small amount of acid.[5]

2.2. Self-assembly

We have also synthesized various coordination polymers from the self-assembly of square-planar Ni(II) or Cu(II) macrocyclic complexes as metal building blocks and carboxylate ligands as organic building blocks at room temperature.[2] In particular, the Ni(II) or Cu(II) macrocyclic complexes act as linear linkers that connect the ligands to form networks whose topologies are solely determined by the ligands (Fig. 4). Contrary to the case of MOFs, in this case, organic ligands are located at the nodes and metal building blocks are at the struts. For example, the self-assembly of Ni(II) or Cu(II) macrocyclic complexes with a ligand of

tetrahedral geometry results in the diamondoid networks.[6,7] In case of trigonal shaped ligand 1,3,5-benzenetricarboxylate (BTC^{3-}), honeycomb or brickwall networks are constructed depending on the solvent system.[8] In this particular case, addition of other solvents such as pyridine changes the coordination mode of the ligand to metal ion, and alters the network structure.

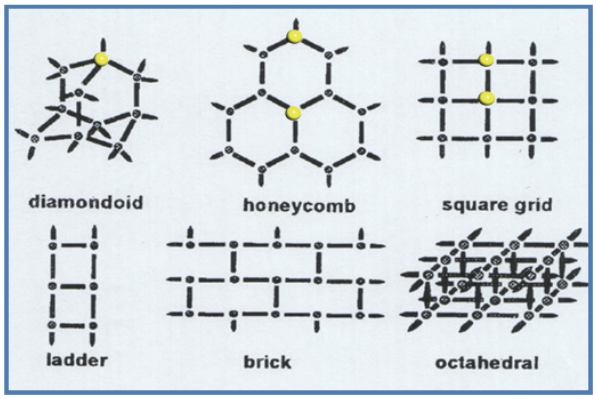

Fig. 4 Self-assembly of organic building blocks and square-planar macrocyclic complexes: Topology of resulting network is determined by the ligand geometry.[2]

3. Properties of MOFs and PCPs

3.1. Flexibility of MOFs and PCPs

Some MOFs and PCPs are highly flexible and responsive to external stimuli. Sometimes, they change their structures on guest removal, guest exchange, and anion exchange by maintaining their single crystallinity, which are called single-crystal to single-crystal transformations. For instance, a bilayer network prepared from bismacrocyclic Ni(II) complex and BTC^{3-} (BTC = 1,3,5-benzenetricarboxylate) ligand exhibited sponge-like behavior, shrinking and swelling depending on the amount of guest solvent molecules included in the networks.[9,10] In addition, this bilayer network maintains their single crystallinity during the guest removal and guest exchange.

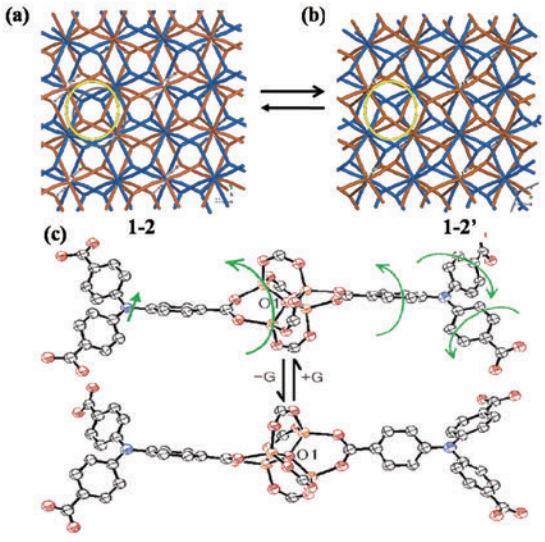

Fig. 5 Reversible transformations of a MOF structure on guest removal and reintroduction. (a) Doubly interpenetrated PdF_2-net of as-synthesized $[Zn_4O(NTB)_2]\cdot 3DEF\cdot EtOH$. (b) Desolvated structure of $[Zn_4O(NTB)_2]$. (c) Rearrangements of the framework structure by the dynamic motions of molecular components.[3]

For the 3D MOF, $[Zn_4O(NTB)_2]\cdot 3DEF\cdot EtOH$ (**1**) (DEF = *N,N'*-diethylformamide), which was prepared from the solvothermal reaction of $Zn(NO_3)_2$ and 4,4',4"-nitrilotrisbenzoic acid (H_3NTB_3) in DEF/EtOH/H_2O (5;3:2, v/v), the pore size and shape changed on guest removal due to dynamic motions of the molecular components, in particular, the rotation of aromatic rings around the Zn_4O metal cluster unit as verified by the single crystal X-ray structure analyses (Fig. 5).[3]

When the guest solvent molecules included between the layers of 2D square-grid coordination polymer $\{[Ni(cyclam)]_2[BPTC]\}_n\cdot 2nH_2O$ are removed, interlayer distances are reduced due to the rotation, sliding, and bending motions of the molecular components via a single crystal to single crystal transformation (Fig. 6).[11]

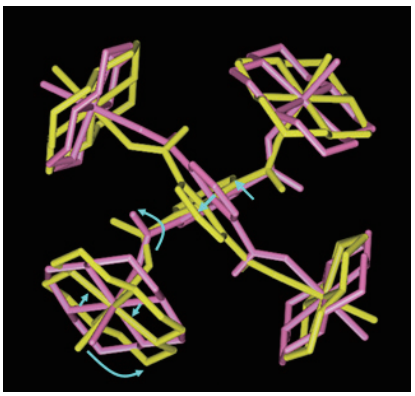

Fig. 6 Dynamic motions of molecular components on removal of guest solvent molecules included between 2D layers.[11]

In a 3D MOF $[Zn_3(NTB)_2(EtOH)_2]_n\cdot 4nEtOH$, ethanol molecules are coordinated at the Zn(II) ion as well as being included in the pores of the MOF. When the coordinated EtOH as well as the guest EtOH molecules were removed by the heat-evacuation method, the coordination geometry of Zn(II) was changed from trigonal bipyramid to tetrahedral by changing the bond angles and bond distances around the metal ions with retention of the single crystallinity of the MOF.[4]

3.2. Responsive Properties of MOFs and PCPs

MOFs are often highly responsive to the external stimuli such as activation methods, temperatures, and external

chemical reagents, and change their structures or oxidation states of metal ions or ligands in the MOFs. For example, when $[Zn_4O(TCBPA)_2]\cdot 19DMA\cdot 4H_2O$ (**SNU-77**), which was synthesized from DMA (*N,N*-dimethylacetamide) solution of $Zn(NO_3)_2\cdot 6H_2O$ and an extended carboxylic acid tris(4-carboxybiphenyl)amine (H_3TCBPA), was activated by the various activation methods such as guest exchange with toluene followed by evacuation at room temperature, direct activation with supercritical CO_2, and evacuation of the guest-exchanged sample at high temperature, it underwent the single-crystal to single-crystal transformations to afford **SNU-77R**, **SNU-77S**, and **SNU-77H**, respectively.[12] These guest free MOFs have different window sizes and shapes as characterized by single crystal X-ray structures (Fig. 7).

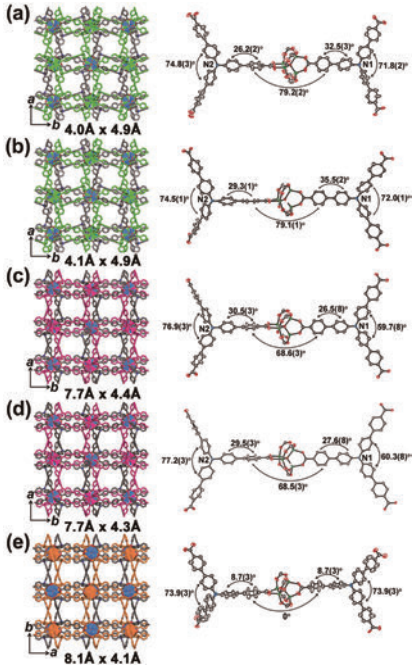

Fig. 7 X-ray crystal structures of (a) **SNU-77**, (b) **SNU-77'**, (c) **SNU-77R**, (d) **SNU-77S**, and (e) **SNU-77H.** Doubly interpenetrated networks are represented in two different colors. The numbers below each figure represent the effective aperture size.[12]

The guest-free structure was also affected by the temperature change as verified by the variable temperature synchrotron X-ray single-crystal analyses (Fig. 8).

Despite the different fine structures, **SNU-77R**, **SNU-77S**, and **SNU-77H** show similar gas sorption properties due to the nonbreathing nature of the framework and an additional structural change upon cooling to cryogenic gas sorption temperature. In particular, **SNU-77H** exhibits high surface area (BET, 3670 m^2g^{-1}), high pore volume (1.52 cm^3g^{-1}), and exceptionally high uptake capacities for N_2, H_2, O_2, CO_2, and CH_4 gases.[12]

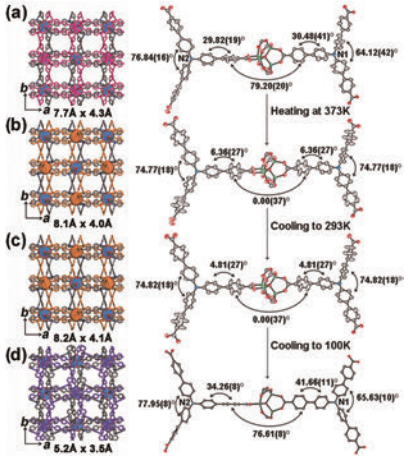

Fig. 8 Structural transformations of **SNU-77R** on sequential temperature changes. (a) at 293 K, (b) 373 K, (c) 293 K (2nd), and then (d) 100 K.[12]

3.3. Ligand exchange

Some MOFs are also responsive to the external organic reagents. For example, when $[Zn_2(TCPBDA)(H_2O)_2]\cdot 30DMF\cdot 6H_2O$ **(SNU-30)** ($H_4TCPBDA$ = *N,N,N',N'*-tetrakis(4-carboxyphenyl)-biphenyl-4,4'-diamine), in which water molecules are coordinated at the paddle wheel SBUs, was immersed in DMF solution of bpta (3,6-di(4-pyridyl)-1,2,4,5-tetrazine) at 80 °C for 3 h, it replaces coordinated water molecules with bpta, which divides the channels of the MOF and results in reduction of the pore sizes.[13] The modified MOF exhibits selective CO_2 adsorption over N_2, O_2, H_2, and CH_4 while desolvated **SNU-30'** adsorbs all gases such as N_2, O_2, H_2, CO_2, and CH_4 gases.

3.4. Guest Ion exchange

MOFs and PCPs that contain guest anions in the pores can undergo ion exchange. By immersion of the solids in the solution of other anion source, the guest anions of the MOFs can be exchanged with external ones since the MOFs recognize the external chemicals as stimuli and response to them. For example, the self-assembly of AgX (X = NO_3^-, $CF_3SO_3^-$, and ClO_4^-) with ethylenediaminetetrapropionitrile (EDTPN, $C_{14}H_{20}N_6$) results in $[Ag(C_{14}H_{20}N_6)(NO_3)]$ (**1**), $[Ag(C_{14}H_{20}N_6)]CF_3SO_3$ (**2**), and $[Ag(C_{14}H_{20}N_6)]ClO_4$ (**3**). Even though compounds **1-3** have the same 1:1 Ag:L stoichiometry, they have topologies of 1D, 2D layer, and a box-like 2D, respectively. When crystal **2** was immersed in the aqueous solutions of $NaNO_3$ and $NaClO_4$, respectively, $CF_3SO_3^-$ anion in **2** was exchanged with NO_3^- and ClO_4^- quantitatively in the crystalline state. The anion-exchange was reversible between **1** and **2** but irreversible from **1** or **2** into **3**. Interestingly, concomitant with the anion exchange, structural transformations underwent in the crystalline states, as evidenced by PXRD

patterns, accompanying the changes in the cell dimensions.[14]

3.5. Redox properties

Some PCPs and MOFs, when they contain redox active metal ions or ligands, are redox active and react with redox agents. For example, the PCPs constructed from Ni(II) macrocyclic complexes are commonly redox active and reduce iodine or metal ions, since Ni(II) macrocyclic species incorporated in the network can be easily oxidized to the Ni(III) species.

A bilayer network, $[Ni_2(C_{26}H_{52}N_{10})]_3[BTC]_4 \cdot 6C_5H_5N \cdot 36 H_2O$, which was self-assembled from Ni(II) bismacrocyclic complex $[Ni_2(C_{26}H_{52}N_{10})(Cl)_4] \cdot H_2O$ and Na_3BTC (BTC =1,3,5-benzenetricarboxylate) in water in the presence of DMSO and pyridine, reacted with iodine to generate networks incorporating mixed valence metal ion species, Ni(II) and Ni(III), and include I_3^- anions in the channels.[15]

Furthermore, the PCPs assembled from Ni(II) macrocyclic complexes and carboxylate ligands reacted with the solutions of metal ions such as Ag(I),[11,16] Au(III),[11] and Pd(II)[7] to generate small (2~4 nm) and monodispersed Ag, Au, and Pd nanoparticles, respectively, in the pores (Fig. 9).[17] These processes occurred in the absence of extra reducing or stabilizing agents, and also without heating or irradiation. In all cases, the structures of PCPs were retained even after the formation of NPs as evidenced by the PXRD patterns.

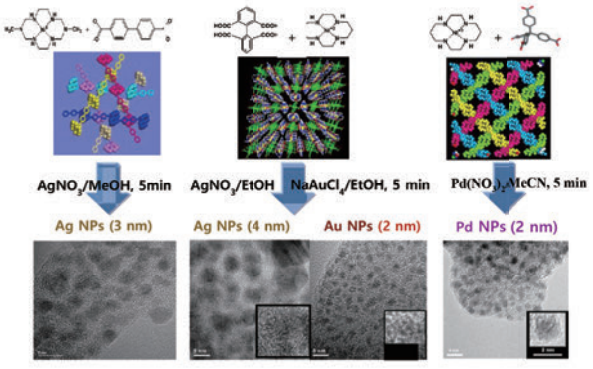

Fig. 9 Fabrication of metal nanoparticles in PCPs by immersion of the redox-active PCPs in the metal ion solutions.[7,11,16]

The MOFs constructed of redox active organic ligands also react with metal ions to afford metal nanoparticles. For example, when $[Zn_3(NTB)_2(EtOH)_2] \cdot 4EtOH$ (EtOH = ethyl alcohol), which was constructed from redox active ligand, 4,4',4"-nitrilotrisbenzoate (NTB^{3-}), was immersed in the MeCN solution of $Pd(NO_3)_2$ for 5 - 30 min, the Pd nanoparticles of size 3.0 ± 0.4 nm were formed in the channels (aperture size, 7.7 Å) of the MOF, and the nitrogen atom of the NTB^{3-} ligands were oxidized to amine radicals. Even after the formation of much bigger Pd NPs than the pore size of the MOF, the structure of the MOF was maintained as evidenced by PXRD data, since the possible maximum destruction of the MOF skeleton by Pd NPs formed was less than 0.7 % by volume according to the calculation.[18]

The advantage of this metal-NPs fabrication method is that the amount of NPs formed in the PCPs or MOFs can be controlled by the immersion time of the solid in the metal ion solutions. Interestingly, the sizes of NPs depend only on the structures of the PCPs, and they are independent of the immersion time, concentration of the metal ion solutions, temperature, and type of the solvent.[17]

3.6. Porosity of MOFs and PCPs

A numerous MOFs and PCPs, which have relatively small to very large surface area, have been reported (Fig. 10). The surface areas of MOFs and PCPs can be easily controlled by the ligand design. In general, when the ligand length is extended, the surface area of the material is increased. For the doubly interpenetrated PdF_2 type networks constructed from the solvothermal reaction of $Zn(NO_3)_2$ with 4,4',4" -nitrilotrisbenzoate (NTB^{3-})[3] and with tris(4-carboxybiphenyl) amine (H_3TCBPA) that contains one more phenyl ring in the branches of the ligand,[12] respectively, the surface area (3670 $m^2 g^{-1}$) of the MOF with the extended ligand ($TCBPA^{3-}$) is significantly greater than that (1120 $m^2 g^{-1}$) of the MOF with NTB^{3-} ligand.[3,12] The same things are generally true with other cases also.[19] The highest BET surface area of MOFs reported so far is 7140 $m^2 g^{-1}$ for NU-110.[20]

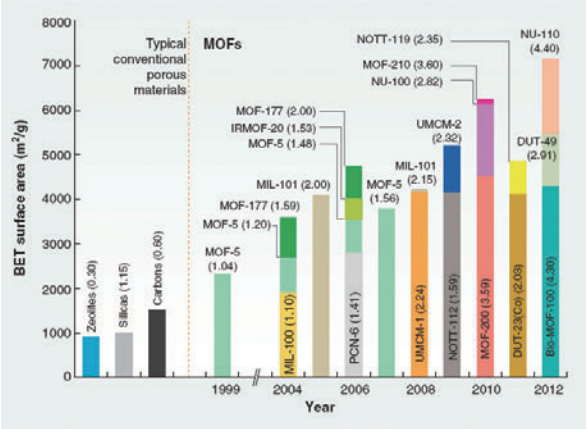

Fig. 10 Porosity of MOFs.[20]

4. Hydrogen Storage in MOFs and PCPs

MOFs and PCPs can store large amount of hydrogen at cryogenic temperature. The hydrogen storage capacities at 77 K generally have a qualitative linear relationship with surface areas of the MOFs, and thus increase with increasing the surface area (Fig.11).[21] The highest H_2 storage capacity reported so far for MOFs is excess 99.5 mg g^{-1} at 77 K and

56 bar with a total capacity of 164 mg g^{-1} at 77 K and 70 bar in **NU-100** that has BET surface area of 6,143 m^2 g^{-1}.[22a] The highest total H_2 storage capacity reported so far is 176 mg g^{-1} (excess 86 mg g^{-1}) at 77 K and 80 bar in **MOF-210**, which has BET surface area of 6240 m^2 g^{-1}.[22b]

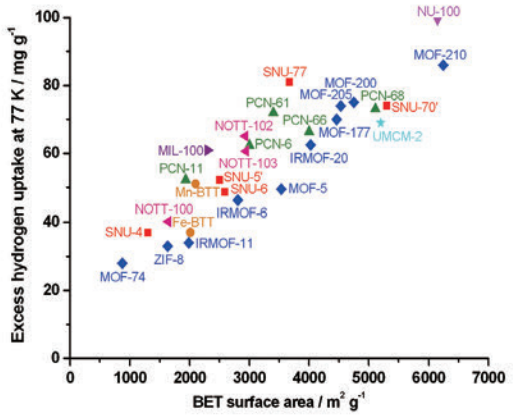

Fig. 11 Excess H_2 storage capacities at 77 K under high pressure vs. BET surface areas of MOFs.[21]

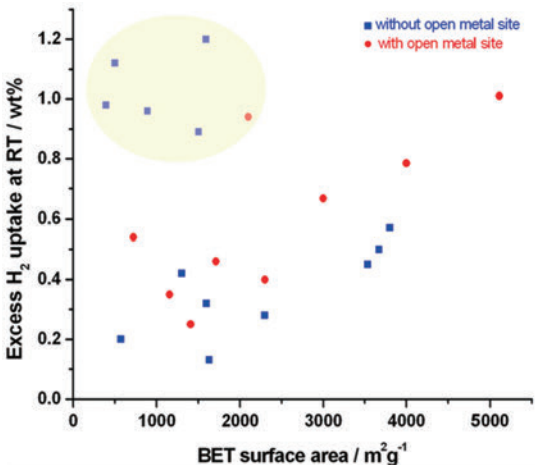

Fig. 12 Room temperature H_2 uptake capacities vs. BET surface areas of MOFs.[21]

Despite that large amounts of H_2 gas can be stored in PCPs and MOFs at low temperatures such as 77 K and 87 K, their H_2 storage capacities at ambient temperature fall down to very low values, ca. 10% of the cryogenic capacities, since the gas adsorption on the pore surfaces of the materials is physisorption and it has very low interaction energy with the adsorbents. The isosteric heats of the H_2 adsorption in common MOFs such as MOF-5 are 4 – 7 kJ mol^{-1}. Furthermore, the room-temperature H_2 storage capacities of MOFs have little relationship with the surface areas of the materials as shown in Fig. 12. Therefore, in order to enhance the gas storage of MOFs at ambient temperature, interaction energies between the materials and H_2 gas should be increased by modifying the pore spaces of the MOFs. We have tried various modification methods such as incorporation of functional groups in the ligand, construction of charged MOFs, generation of accessible metal sites, embedding metal nanoparticles (NPs) in the MOF, inclusion of specific metal ions or organic molecules as guests, and incorporation of specific cation binding sites in the framework.

4.1. Hydrogen storage in MOFs incorporating functional groups in the ligands

Incorporation of functional groups in the ligand requires elaborate synthetic works, but the effects on H_2 storage are rather minor. By synthesizing *N*,*N*'-bis(3,5-dicarboxyphenyl) pyromellitic diimide (H_4BDCPPI) as an organic building block, we prepared 3D MOFs, $\{[Cu_2(BDCPPI)(DMF)_2]\cdot 10DMF\cdot 2H_2O\}_n$ (**SNU-50**) and $\{[Zn_2(BDCPPI)(DMF)_3]\cdot 6DMF\cdot 4H_2O\}_n$ (**SNU-51**) (Fig. 13).[23] Despite that the desolvated solid $[Cu_2(BDCPPI)]_n$ (**SNU-50'**) contains vacant coordination sites at the metal ions as well as functional groups in the ligand, it adsorbs 2.10 wt% of H_2 at 1 atm and 77 K, and total 7.85 wt% of H_2 at 77 K and 60 bar. Activated sample of **SNU-51** does not adsorb any gas, independent of the activation temperature, due to collapse of the framework. The isosteric heat of the H_2 adsorption in **SNU-50'** is 7.1 kJ mol^{-1}, which is only ca. 2-3 kJ mol^{-1} higher than those of the common MOFs.

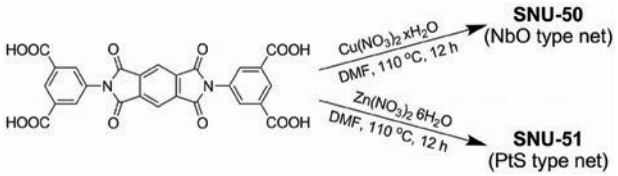

Fig. 13 Synthesis of MOFs by using N,N'-bis(3,5-dicarboxyphenyl) pyromellitic diimide (H_4BDCPPI).[23]

4.2. Hydrogen storage in MOFs with accessible metal sites

This method is based on "Kubas" interaction of hydrogen molecule with a metal ion, which involves donation of the σ-orbital electron of dihydrogen to metal and π-backdonation of the metal electron to σ*-orbital of dihydrogen. In MOFs, metal ions in paddle-wheel type SUBs are commonly coordinated with solvent molecules, which can be removed by activation to generate accessible metal sites (AMSs). Thus formed AMSs can directly interact with hydrogen molecules, resulting in stronger interactions between the MOF and hydrogen.

For example, two porous MOFs having the same NbO-net topology, $[Zn_2(ABTC)(DMF)_2]_3\cdot 4H_2O\cdot 10DMF$ (**1**) and $[Cu_2(ABTC)(H_2O)_2]_3\cdot 10DMF\cdot 6$(1,4-dioxane) (**2**), were synthesized from the solvothermal reactions of H_4ABTC (1,1'-azobenzene-3,3',5,5'-tetracarboxylic acid)

with $Zn(NO_3)_2 \cdot 6H_2O$ in DMF at 100°C for 12 h and with $Cu(NO_3)_2 \cdot xH_2O$ in DMF/1,4-dioxane/H_2O (4:3:1 v/v) at 80°C for 24 h, respectively.[24] By activating the MOFs under the precisely controlled conditions, $[Zn_2(ABTC)(DMF)_2]_3$ (**1a**) and $[Cu_2(ABTC)(DMF)_2]_3$ (**2a**) with no AMS, and $[Cu_2(ABTC)]_3$ (**2b**) with AMSs were obtained. The framework structure of **1a** was the same as that of **1**, and those of **2a** and **2b** were same as that of **2**, as evidenced by the PXRD patterns. The MOF (**2b**) with AMSs adsorbed 2.87 wt% of H_2 gas at 77 K and 1 atm, which was significantly higher than the other two MOFs having no AMS (2.07 wt% for **1a** and 1.83 wt% for **2a).** The excess H_2 uptake of **2b** at 77 K and 50 bar is 5.22 wt% (total 6.76 wt%), which is much higher than 3.70 wt% (total 4.49 wt%) in **1a**. This enhancement is mainly due to the reduced mass effect by removal of the coordinated solvent molecules**.** The volumetric H_2 storage capacity is also enhanced by the presence of AMSs; volumetric storage ratios of **2b**:**1a** and **2b**:**2a** at 77 K and 1 atm are 105% and 120%, respectively, and that of **2b**:**1a** at 77 K and 40 bar is 117%. Furthermore, the zero coverage isosteric heat of H_2 adsorption in the MOF with AMSs reached to 11.7 KJ mol^{-1}, which is significantly higher than those of the other two, 7.24 kJ mol^{-1} and 6.53 kJ mol^{-1}, respectively. Therefore, it is evident that the MOF with AMSs enhances H_2 adsorption in wt% as well as by per volume of sample (gL^{-1}) via offering the stronger interaction with H_2 molecules, although its reduced mass is the major contribution in higher wt% for the H_2 uptake (Fig. 14).

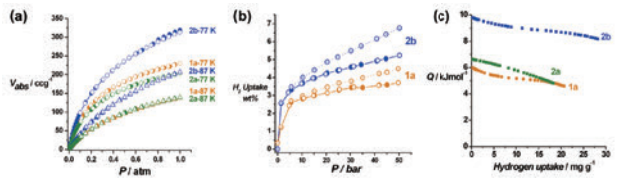

Fig. 14 (a) H_2 gas sorption isotherms at 77 K (●) and 87 K (▲) up to 1 atm H_2 for 1a (orange), 2a (green), and 2b (blue). (b) Excess (—) and total (- - -) H_2 adsorption isotherms at high pressures and 77 K. Filled shape, adsorption; open shape, desorption. (c) Isosteric heat of H_2 adsorption for 1a (orange), 2a (green), and 2b (blue).[24]

4.3. Hydrogen storage in a MOF embedded with palladium nanoparticles

To enhance hydrogen storage, metal nanoparticles that strongly bind hydrogen have been fabricated in MOFs or PCPs. As mentioned previously, we have developed a simple method for fabricating metal nanoparticles in MOFs and PCPs without using extra reducing agent or NP-stabilizing agent just at room temperature, based on the redox chemistry between the redox-active components of the MOFs or PCPs and the external metal ions.

By simple immersion of the redox active MOF, $[Zn_3(NTB)_2(EtOH)_2] \cdot 4EtOH$ (EtOH = ethyl alcohol), which incorporates redox-active ligand 4,4',4"-nitrilotrisbenzoate (NTB^{3-}), in the MeCN solution of $Pd(NO_3)_2$ for ca. 5 -30 min, Pd NPs (size: 3.0 ± 0.4 nm) were fabricated in the pores of the MOF.[18] The amount of Pd loaded in the MOF was controlled by the immersion time of the MOF in the Pd(II) solution, which affected hydrogen uptake capacity of the MOF. In case of 3 wt% Pd NPs loaded MOF, H_2 adsorption was enhanced by 350% at 77 K and 1 atm, and by 230% at room temperature and high pressures. Solid Pd NPs(3 wt%)@[**SNU-3**]$^{x+}(NO_3^-)_x$ exhibited selective gas sorption properties for CO_2 and H_2 gases over N_2, implying its potential application in gas separation processes also.

4.4. Hydrogen storage in a MOF embedded with magnesium nanocrystals

To combine a MOF, which physisorbs hydrogen, with a material that chemisorbs great amounts of hydrogen, we have fabricated magnesium (Mg) NPs in the pores of a MOF.[25] **SNU-90** was synthesized from $Zn(NO_3)_2$ and aniline-2,4,6-tribenzoic acid, which showed BET surface area of 4240 m^2 g^{-1} and pore size of 1.25 nm. First, chemical vapour of $MgCp_2$ was deposited to the activated MOF to afford $Mg(Cp)_2$@ SNU-90'. And then, it was heated at 200 °C under argon atmosphere to afford the MOF embedded with hexagonal disk shaped magnesium nanocrystals with size of av. 60 ± 18 nm and thickness of av. 37 ± 12 nm (Fig.15).

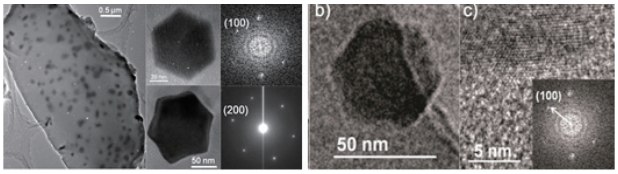

Fig. 15 High resolution transmission electron microscopy (HRTEM) images of Mg@SNU-90'. On exposure to air, Mg nanocrystal changes to a star shape.[25]

By changing the reaction conditions of vapor deposition process of $Mg(Cp)_2$, various amounts of $Mg(Cp)_2$ could be loaded in the MOF, which resulted in the MOFs embedded with various amounts of Mg nanocrystals (NCs). The MOFs impregnated with Mg nanocrystals show the same PXRD patterns as that of the pristine MOF, since only less than 4.6% of MOF's skeleton by volume can be destroyed according to calculation, even if all Mg NCs would destroy the MOF framework. As the amount of Mg embedded in the MOF increases, the BET surface area, pore volume, and H_2 uptake

capacity at 77 K and 87 K under 1 atm decrease because Mg NCs occupy the surface and pore space of the MOF. At 298 K and high pressure, however, the H_2 uptake in Mg(1.26 wt%)@**SNU-90'** increases by 20%, compared to that of pristine **SNU-90',** suggesting that the Mg NCs provide a positive effect on H_2 adsorption at 298 K. Importantly, the zero-coverage isosteric heat of the H_2 adsorption increases as the amount of Mg increases, up to 11.6 kJ mol^{-1} for Mg(10.5 wt%)@**SNU-90'** from 4.55 kJ mol^{-1} for **SNU-90'** (Table 1, Fig. 16).

Contrary to hydrogen physisorption, hydrogen chemisorption increases as the amount of Mg NCs loaded in the MOF increases. At 473 K under 30 bar, the H_2 uptake capacity of Mg(10.5 wt%)@**SNU-90'** became 0.71 wt% (volumetric H_2 storage capacity, 3.1 g L^{-1}), which is remarkably higher than that (0.29 wt%) of Mg(6.5 wt%)@**SNU-90'** under the same conditions (Table 1), despite that the former exhibits much lower surface area and pore volume. As for the chemisorption temperatures, 10.5 wt% Mg loaded sample starts to absorb H_2 at 50 °C, which is ca. 450 °C lower than the temperature of the H_2 chemisorption in the bulk magnesium. Furthermore, contrary to the physisorption, the H_2 chemisorption in Mg@**SNU-90'** increases as the temperature is raised. The chemisorption temperatures of the present materials are significantly lower (by > 200 K) than that (673 K under 10 bar) of bare Mg powder ranging 50 - 100 μm in size.[26] On estimation from the hydrogen chemisorption data, the H_2 absorption in Mg alone is 7.5 wt% at 473 K and 30 bar, indicating that more than 90% of Mg NCs in the sample absorbs H_2. This is much greater than any form of Mg previously reported, such as Mg nanoparticles incorporated in a polymer[27] or bare Mg powder.[28] The H_2 desorption properties of Mg@**SNU-90'** examined by the temperature programmed desorption mass spectroscopy (TPD-MS) analysis indicates that H_2 can be desorbed at T > 523 K and 1 atm. In short, Mg NCs@**SNU-90'** stores hydrogen by physical adsorption at low temperatures (< 25 °C) and by chemisorption at high temperatures (> 50 °C). It offers synergistic effects on both physic- and chemi- sorption of H_2, increasing the isosteric heat of H_2 physisorption by ca. 7 kJ mol^{-1} and uptake capacity at 298 K and 80 bar by 20%, and decreasing the chemisorption/desorption temperatures by 200 K as well as converting more than 90% of Mg to MgH_2.

Table 1 Hydrogen adsorption data in a MOF impregnated with Mg nanocrystals.[25]

compound	Mg/Zn mol/mol (wt%)	N_2 uptake $cm^3 g^{-1}$	surface area $m^2 g^{-1}$	H_2 uptake, wt% at 1 atm	H_2 uptake, wt% at high pressures (condition)	Q_{st} kJ mol^{-1}
SNU-90'	N/A	1135	4244[a]	1.21 (77 K) 0.74 (87 K)	8.81 (77 K, 75 bar) 0.45 (298 K, 80 bar)	4.55
Mg(1.26 wt%)@**SNU-90'**	0.15 (1.26)	1104	4154[a]	1.24 (77 K) 0.65 (87 K)	8.74 (77 K, 89 bar) 0.54 (298 K, 90 bar)	5.68
Mg(6.52 wt%)@**SNU-90'**	0.85 (6.52)	559	2056[a]	0.72 (77 K) 0.40 (87 K)	0.29 (473 K, 30 bar)	7.24
Mg(10.5 wt%)@**SNU-90'**	1.40 (10.5)	378	1371[a]	0.60 (77 K) 0.47 (87 K)	0.20 (323 K, 80 bar) 0.24 (415 K, 40 bar) 0.71 (473 K, 30 bar)	11.6

4.5. Hydrogen storage in a MOF including crown ether guests

We expected that inclusion of 18-crown-6 (18C6) or 15-crown-5 (15C5) in a MOF would increase the hydrogen uptake in the MOF, since the oxygen atoms of crown ether posses the partial charge of -0.47 ~ -0.48 according to our calculation.[29] We included 18C6 and 15C5, respectively, in the MOF that was synthesized from benzophenone-4,4'-dicarboxylic acid (H_2BPnDC), 4,4'-bipyridine (bpy), and $Cu(NO_3)_2 \cdot 2.5H_2O$.[30] The MOF has pore size that is big enough to accommodate the crown ether molecules. By immersing the MOF in the solutions of a crown ether with various concentrations, various amounts of 18C6 and 15C5, respectively, were included in the MOF.[29] The hydrogen uptake capacity in the MOF was decreased as the amount of crown ether inclusion increases. However, the isosteric heats (Q_{st}) of the H_2 adsorption in the MOF was increased to 10.4 kJ mol^{-1} and to 9.07 kJ mol^{-1} upon inclusion of 18C6 and 15C5, respectively, compared with 7.74 kJ mol^{-1} for the pristine MOF. These enhancements by 2.7 kJ mol^{-1} and 1.3 kJ mol^{-1}, respectively, are comparable to the effect of the accessible metal sites in the MOFs, and much greater than the effect of the inclusion of alkali metal or alkaline earth metal ions in the MOFs, which enhances Q_{st} values by ca. 0.2 - 1.1 kJ mol^{-1}.[31-35]

4.6. Hydrogen storage in a MOF incorporating specific metal binding sites

In **o**rder to con**s**truct a MOF that adsorbs hydrogen molecules with stronger interaction energy than the common MOFs, a MOF incorporating 18C6 moiety in the struts has been prepared.[36] $[Zn_5(\mu_3\text{-}OH)_2(TBADB\text{-}18C6)_2 \cdot 4DMF] \cdot 13DMF \cdot 12H_2O$ (**SNU-200**, TBADB-18C6 = 4,4',5,5'-terabenzoic acid dibenzo-18-crown-6, DMF = *N*,*N*-d*i*methylformamide) binds K^+, NH_4^+, and methyl viologen (MV^{2+}) cations in the cavity of 18C6 moiety, and includes the counter anions in the pores, via the single-crystal to single-crystal transformation. The samples were activated with supercritical CO_2. Even after binding of cations and anions (K^+, NH_4^+, MV^{2+}/Cl^-, SCN^-), the surface area of the MOF did not decrease, compared to that of as-synthesized **SNU-200**. The material exhibits a higher isosteric heat (Q_{st}) of the H_2 adsorption (7.70 kJ mol^{-1}) than the common Zn based MOFs due to the partial charge of the oxygen atoms in 18Cr6 moiety.

Among K^+, NH_4^+, and MV^{2+} bound SNU-200 analogues, the K^+/SCN^- bound MOF shows the most highly enhanced isosteric heat (Q_{st}) of the H_2 adsorption (9.92 kJ mol^{-1}) because of the presence of the accessible metal sites on K^+ cations that directly interact with H_2 molecules.[36]

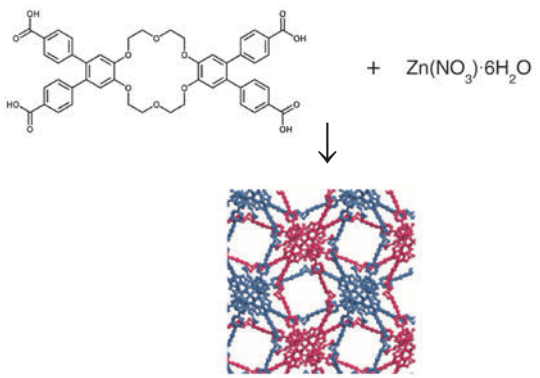

Fig. 16 Synthesis of the MOF incorporating a crown ether moiety in the struts.[36]

5. Carbon Dioxide Capture in MOFs and PCPs

Every year, ca. 30 Giga tons of carbon dioxide (CO_2) are emitted worldwide, of which 60-70% is originated from the power plant and industry. In order to mitigate the recent environmental crises such as global warming and ocean acidification, efficient CO_2 capture technologies should be developed. The MOFs and PCPs may be the excellent candidate materials for CO_2 capture from the power plant exhaust. Typical post-combustion flue gas from a coal-fired power plant contains N_2 (73-77%), CO_2 (15-16%), H_2O (5-7%), and other gases such as O_2 (3-4%), SO_2 (800 ppm), SO_3 (10 ppm), NO_x (500 ppm), HCl (100 ppm), CO (20 ppm), and hydrocarbon (10 ppm), with the emission temperature of 313 ~ 343 K and the emission pressure of 1 atm. Therefore, the materials for CO_2 capture from the flue gas should have a high adsorption selectivity of CO_2 over N_2 at a low CO_2 partial pressure (ca. 0.15 atm) and a high CO_2 uptake capacity at elevated temperatures as well as an outstanding water stability, fast adsorption and desorption kinetics, and an excellent regenerability.

5.1. Strategies of carbon dioxide capture by using flexible MOFs and PCPs.

To capture CO_2 selectively from the flue gas by using porous solids, we designed highly flexible 3D PCPs and MOFs whose channels or pores might open and close depending on the gas type, temperature, and pressure (Fig. 17). We expected that CO_2 would interact with the host network much more strongly than other gases because of the higher quadrupole moment (1.34 x 10^{-39} Cm^2) and polarizability (2.63 x 10^{-24} cm^3) of CO_2, and opens up the windows of flexible PCPs, which are closed for other gases (Fig.17).

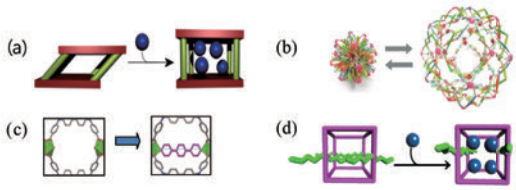

Fig.17 Several strategies for capturing CO_2 by using flexible PCPs and MOFs.

5.2. Selective CO_2 capture by the 3D PCPs having flexible pillars

Two flexible 3D PCPs with very small pores, $[(Ni_2L^2)(BPTC)]\cdot 6H_2O\cdot 3DEF$ and $[(Ni_2L^4)(BPTC)]\cdot 14H_2O$, were self-assembled from Ni(II) bismacrocyclic complexes linked with flexible ethyl and butyl groups, respectively, and 1,1'-biphenyl-3,3',5,5'-tetracarboxylate ($BPTC^{4-}$) as shown in Fig. 18.[37]

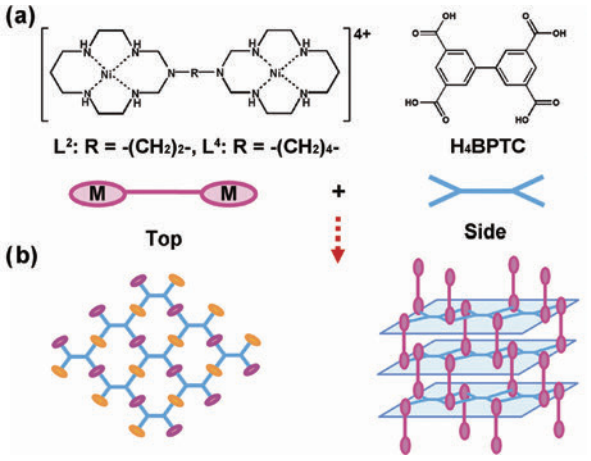

Fig. 18 (a) Alkyl-bridged Ni(II) bismacrocyclic complexes and H_4BPTC. (b) Construction of 3D PCPs from 2D layers and alkyl pillars. Bismacrocyclic complexes located upward and downward with respect to a 2D plane are indicated by the different colors.[37]

The X-ray crystal structures indicate that the resulting 3D PCPs, $[(Ni_2L^2)(BPTC)]\cdot 6H_2O\cdot 3DEF$ and $[(Ni_2L^4)(BPTC)]\cdot 14H_2O$, are consisted of 2D coordination polymers and highly flexible alkyl pillars, ethyl and butyl pillars, respectively. The 2D grids are constructed of square-planar Ni(II) macrocyclic complex as a linear linker and $BPTC^{4-}$ as a square-shape organic building block. The alkyl pillars are highly tilted. Interestingly, butyl pillars are much more tilted (68.4°) than the ethyl pillars (40.5°).

The activated PCPs having ethyl and butyl pillars, **SNU-M10** and **SNU-M11**, respectively, hardly adsorb N_2, H_2,

and CH_4 gases even at low temperatures, but they adsorb CO_2 selectively (Fig. 19). The materials have thermal stability up to 300 °C, and air- and water- stability. The CO_2 adsorption isotherms show gate opening and closing phenomena. The gate opening pressure increases as the temperature increases. The gate opening pressure of **SNU-M11** at 298 K is ca. 20 bar, which is much higher than the CO_2 partial pressure of flue gas, and thus the material cannot be applied in post combustion CO_2 capture.

Contrary to **SNU-M11**, **SNU-M10** uptakes high amount of CO_2 at 298 K (9.2 wt%, 47.2 cm^3g^{-1}, 2.1 $mmolg^{-1}$ at STP at 1 atm), and shows high CO_2/N_2 selectivity (98:1) at 298 K. Although **SNU-M10** is a highly efficient CO_2 capture material, some problems should be still solved before the practical applications, such as lowering the cost of the material and developing the mass production method.

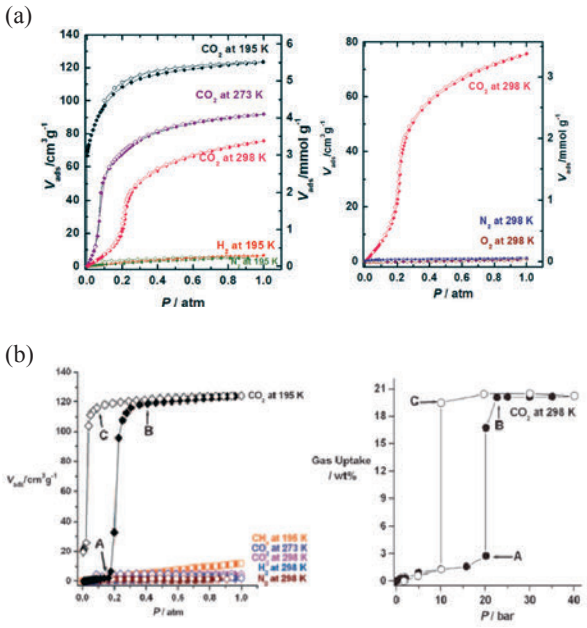

Fig. 19 CO_2 adsorption isotherms of SNU-M10 (a) and SNU-M11 (b).[37]

2.3. Selective CO_2 capture by the MOFs constructed from flexible organic building blocks

A flexible non-interpenetrated 3D MOF, $\{[Cu_2(TCM)(H_2O)_2]\cdot 7DMF\cdot 3(1,4\text{-dioxane})\cdot MeOH\}_n$ (**SNU-21**), was prepared from the solvothermal reaction of flexible organic building block, tetrakis[4-(carboxyphenyl)oxamethyl]methane (H_4TCM) and $Cu(NO_3)_2\cdot 2.5H_2O$ in DMF/1,4-doxane/MeOH (Fig. 20a).[38] The paddle-wheel type $\{Cu_2(O_2CR)_4\}$ building units are connected by TCM^{4-} tetrahedral building blocks to afford a PtS type framework that generates 3D channels. The MOF was activated by two different methods, the supercritical CO_2 treatment and the heat-evacuation, which resulted **SNU-21S** and **SNU-21H**, respectively. Although they have same chemical formula, $[Cu_2(TCM)]_n$, by losing the coordinated water molecules as well as guest solvent molecules, **SNU-21S** showed higher sorption capacities than **SNU-20H** for N_2, O_2, H_2, CH_4, and CO_2 gases as well as higher isosteric heats of gas adsorption, indicating that supercritical CO_2 activation method is superior to the heat-evacuation method. The PXRD patterns indicate that it is associated with the different structural transformations of the flexible framework during the different activation processes. **SNU-21H** and **SNU-21S** show selective and reversible CO_2 capture abilities at room temperature, with the CO_2 adsorption capacities of 9.65 wt% and 11.1 wt% at 1 atm, respectively. Their CO_2(0.15 atm)/N_2(0.85 atm) selectivities at 298 K and 1 atm are 10.6 for **SNU-21H** and 15.5 for **SNU-21S**.

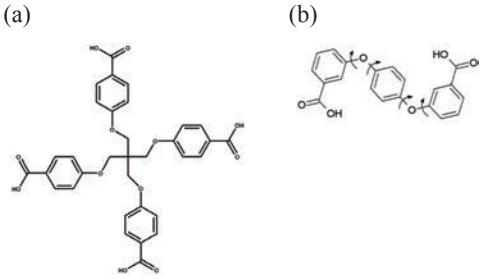

Fig. 20 Flexible organic building blocks. (a) tetrakis[4-(carboxyphenyl)oxamethyl methane (H_4TCM). (b) 3,3'-(1,4-phenylenebis(oxy))dibenzoic acid (H_2*mpm*-PBODB).

In order to capture CO_2 at room temperature, the material should have optimum flexibility, since not all flexible MOFs or PCPs capture carbon dioxide selectively at room temperature. For example, we prepared a flexible MOF $\{[Zn_2(mpm\text{-}PBODB)_2bpy]\cdot 3DMF\}_n$ (**SNU-110**) by using an organic ligand containing flexible joints, 3,3'-(1,4-phenylenebis(oxy)) dibenzoic acid (H_2*mpm*-PBODB) (Fig. 20b).[39] The desolvated solid $[Zn_2(mpm\text{-}PBODB)_2bpy]_n$ (**SNU-110'**) resulted by activation of **SNU-110** with supercritical CO_2 fluid hardly adsorbs N_2 and H_2 gases at 77 K, indicating that it has smaller window size than the kinetic diameter (2.89 Å) of H_2. However, the material uptakes 97 $cm^3\ g^{-1}$ of CO_2 at 195 K despite that CO_2 has much larger kinetic diameter than H_2, indicating that CO_2 can open up the window of the MOF due to its high quadrupole moment and polarizability. **SNU-110'** shows a two-step CO_2 adsorption curve related with structural transformation by CO_2 adsorption, together with a big desorption-hysteresis (Fig. 21). The selectivity for CO_2 adsorption over N_2, H_2, and CH_4 at 195 K is 35:1, 61:1, and 15:1, respectively. However, this material hardly adsorbs CO_2 at 298 K, and thus cannot be applied in practical carbon

capture from the industrial flue gas. The result demonstrates that the material should have optimum flexibility to allow CO_2 to open up its windows at room temperature.

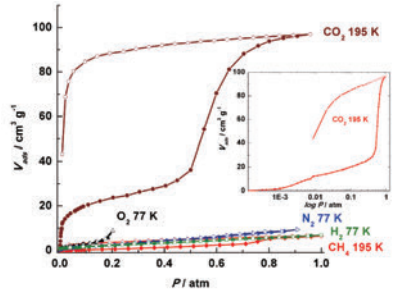

Fig. 21 Gas adsorption isotherms of **SNU-110'**. Inset: CO_2 adsorption at 195 K versus *log P*. Filled shapes: adsorption, open shapes: desorption.[39]

5.4. Selective CO_2 capture by modifying a MOF with flexible carboxyl pendants

Another strategy of developing MOFs for CO_2 capture application was to introduce flexible carboxyl pendants exposed to the channels of the MOFs. For this, a stable MOF, UiO-66, was modified by the post-synthetic ligand exchange. The terephthalate ligand in UiO-66 was exchanged with a series of alkanedioic acids ($HO_2C(CH_2)_{n-2}CO_2H$) to afford the MOFs incorporating various flexible carboxyl pendants (UiO-66-AD*n*: n = 4, 6, 8, and 10, where n denotes the number of carbons in a pendant).[39] The ligand substitution occurred partially, and the extent of ligand exchange depended on the immersion time of the MOF in the solution of alkanedioic acid. The NMR, IR, PXRD, TEM, and mass spectral data suggested that one terephthalate linker in UiO-66 was substituted with two alkanedioates to afford free carboxyl pendants in the pores. The analysis of NMR spectra of the samples that were partially digested by adjusting the amount of acid indicated that the ratio of alkanedioic acid/terephthalic acid increased with the lesser amount of acid, indicating that the ligand substitution proceeded from the outer layer of the MOF particle.

Although N_2 gas adsorption data indicated that the surface area and the pore volume of all UiO-66-AD*n*s were decreased compared to those of UiO-66 and the CO_2 adsorption capacities of UiO-66-AD*n* (n = 4, 8) were similar to that of UiO-66, the CO_2 uptake of UiO-66-AD6 was most highly increased among the samples, by 34% at 298 K and by 58% at 323 K, compared to those of UiO-66 (Fig. 22). The IAST (ideal adsorption selectivity theory) selectivity of CO_2 adsorption over CH_4 was enhanced for all UiO-66-AD*n*s compared to that of UiO-66 at 298 K (Fig. 23). In particular, UiO-66-AD6 with adipic acid pendants showed the most highly increased selectivity of CO_2 over CH_4 at ambient temperature, suggesting that it is a promising material for CO_2 separation of landfill gas.

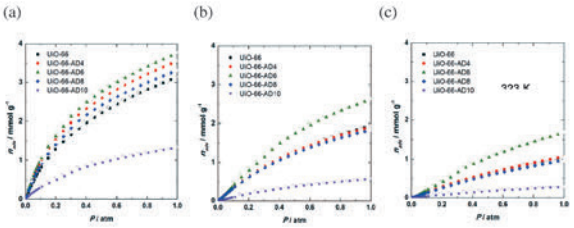

Fig. 22 CO_2 adsorption isotherms at a) 273 K, b) 298 K, and c) 323 K for UiO-66 (■), UiO-66-AD4 (●), UiO-66-AD6 (▲), UiO-66-AD8 (◆), and UiO-66-AD10 (★). Filled shapes: adsorption; open shapes: desorption.[39]

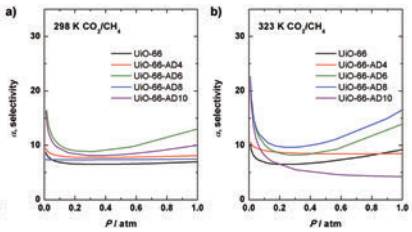

Fig. 23 Estimated IAST selectivity of the CO_2 adsorption from the mixture of CO_2:CH_4 = 50:50 at (a) 298 K, and (b) 323 K.

5.5. CO_2 capture in anionic MOF impregnating metal cations

Similarly to hydrogen storage in MOFs, we expected that impregnation of proper guest molecules in the pores of MOFs, such as charged metal ions, would increase the interaction energy between the materials and CO_2 gas molecules, enhancing the CO_2 uptake capacity and adsorption selectivity. We synthesized an anionic MOF, $[Zn_3(TCPT)_2(HCOO)][NH_2(CH_3)_2]\cdot 5DMF$ (**SNU-100**, TCPT = 2,4,6-tris-(4-carboxyphenoxy)-1,3,5-triazine), by heating the DMF solution of $Zn(NO_3)_2\cdot 6H_2O$ and H_3TCPT at 90 °C for 24 h. The $NH_2(CH_3)_2^+$ cations included in the pores of **SNU-100** were exchanged with various metal ions such as Li^+, Mg^{2+}, Ca^{2+}, Co^{2+}, and Ni^{2+}.[40] The metal ions still coordinating water molecules even after the activation significantly enhanced uptake capacity, selectivity, and the isosteric heat of the CO_2 adsorption while it affects rather slightly the H_2 and CH_4 adsorption (Fig. 24). This is attributed to the electrostatic interactions between the extra-framework metal ions and CO_2. The CO_2 adsorption capacity at 298 K and 1 atm reached to 16.8 wt% in of **SNU-100'-Co**, and the adsorption selectivity of CO_2 over N_2 at room temperature and the isosteric heats of CO_2 adsorption increased to 40.4 and 37.4 kJ mol^{-1}, respectively, in **SNU-100'-Ca**, compared with 14.1 wt%, 25.5, and 29.3 kJ mol^{-1} for the parent MOF (**SNU-100'**).

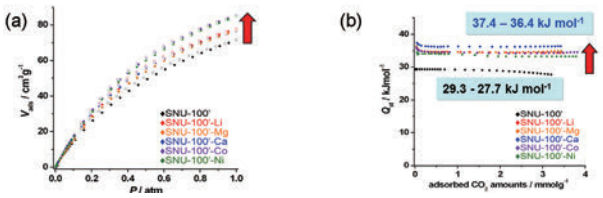

Fig. 24 (a) CO_2 adsorption isotherms at 298 K for anionic MOF including various metal cations in the pores **(SNU-100'-M)**. Filled shapes: adsorption. Open shapes: desorption. (b) Q_{st} of CO_2 adsorption.[40]

5.6. CO_2 capture by porous organic polymer impregnating flexible polymeric amine

As a similar strategy for capturing CO_2 by using flexible MOFs with very small pores, we chose a porous organic polymer, PAF-5, which has BET surface area of 2070 m^2 g^{-1} and large pore size of 2.11 nm, and blocked its pores with a flexible polyethylenimine (Fig. 25).[41] We believed that when flexible polymer PEI units blocked the windows of PAF-5, the material would hardly adsorb N_2 gas while adsorbing CO_2 since it would allow CO_2 to open up the closed windows because of the high polarizability and quadrupole moment of CO_2. In addition, numerous amine functional groups in PEI would strongly interact with CO_2, which increase the capacity and the selectivity of CO_2 adsorption.

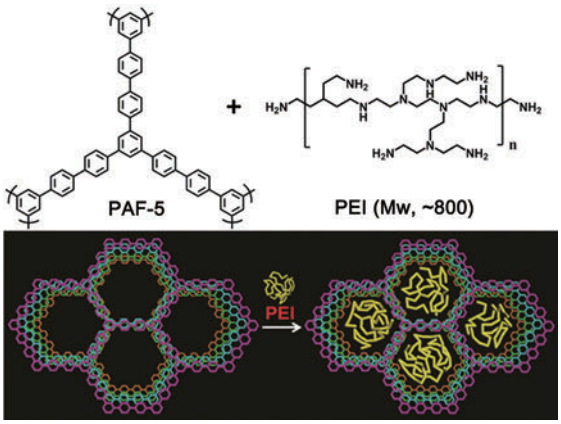

Fig. 25 PAF-5 impregnated with branched PEI (Mw = ca. 800).[41]

By changing the concentration of PEI in MeOH as well as the immersion time of PAF-5 in the PEI solution, we prepared 10, 30, 40 wt% PEI loaded samples. Interestingly, the impregnated PEI was not released even by the activation under the high vacuum due to the C-H···π interactions between the ethylene groups of PEI and phenyl rings of PAF-5. The N_2 uptake at 77 K decreases as the amount of PEI increases, and 40 wt% PEI loaded sample hardly adsorbs N_2 gas. The BET surface area and the pore volume of 40 wt% PEI loaded sample became 40 m^2 g^{-1} and 0.046 cm^3 g^{-1}, respectively, which are only 2% and 3% of those for the pristine PAF-5. Contrary to N_2 adsorption, CO_2 adsorption increases as the amount of PEI increases (Fig. 26). In addition, while pristine PAF-5 shows linearly increasing CO_2 adsorption isotherm and adsorbs only small amount of CO_2 at 0.15 atm of CO_2, the PEI-loaded samples exhibit type-I curves to increase their CO_2 uptake capacities drastically at low CO_2 pressure. Therefore, for the PEI-loaded adsorbents, a sharp increase in the CO_2 uptake at low CO_2 pressure (0.15 atm) together with the big decrease in the N_2 adsorption drastically enhances the adsorption selectivity of CO_2 over N_2. In particular, PEI(40 wt%)⊂PAF-5 adsorbs 10, 14, and 16 times greater amount of CO_2 than pristine PAF-5 under 0.15 atm of CO_2 pressure at 298 K, 313 K, and 323 K, respectively. The CO_2/N_2 (15:85) adsorption selectivity of PEI(40 wt%)⊂PAF-5 reached to 2160 at 313 K, which is the highest value reported so far.

The plot of Q_{st} values versus CO_2 uptake shows two distinctive regions. The first region at low CO_2 loading reaches to ca. 70 kJ mol^{-1}, and the second region at the higher CO_2 loading falls down to ca. 20 kJ mol^{-1}. Interestingly, as amount of PEI increases, the first region covers broader range of CO_2 uptake, indicating that it corresponds to chemisorption of CO_2 on PEI and the second region to physisorption on the surface of PAF-5.

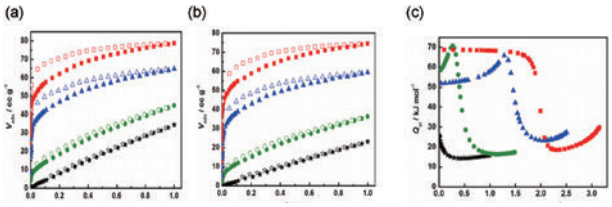

Fig. 26 Gas sorption properties of PAF-5 (★), PEI(10 wt%)⊂PAF-5 (●), PEI(30 wt%)⊂PAF-5 (▲), and PEI(40 wt%)⊂PAF-5 (■). (a) N_2 at 77 K. (b) CO_2 at 313 K. (c) Isosteric heat of CO_2 adsorption. Filled shapes: adsorption process; Open shapes: desoprtion process.[41]

The material PEI(40 wt%)⊂PAF-5 shows high CO_2 uptake capacity (11.1 wt% at 313 K under 0.15 atm of CO_2), high adsorption selectivity (2160 at 313 K) for CO_2/N_2 (15:85), fast adsorption and desorption kinetics (within 10 min.), water stability, and yet low energy penalty for regeneration of the adsorbents (413 K with 11.1 wt% working capacity). Therefore, it is a promising material for the practical application in CO_2 capture from flue gas, once several problems still left are solved, such as cost down of the material and development of large scale up methods.

6. Summary and Prospects

Metal-organic frameworks (MOFs) and porous coordination

polymers (PCPs) are formed by the connectivity of metal and organic building blocks. We have synthesized various MOFs and PCPs by solvothermal reactions and self-assembly, and explored their characteristic properties such as flexibility, responsiveness to external stimuli, selective binding of guest molecules, and redox properties. The MOFs and PCPs have large pore surface areas and relatively low density, and thus they are the good candidates for the materials that can be applied in gas storage and gas separation, in particular, hydrogen storage and carbon dioxide capture. However, the gas sorption in these materials is physisorption, and it has very weak interaction energy with the gas. Therefore, their gas sorption capacities fall down to very low values as the temperature is elevated to that of practical applications. Therefore, to enhance gas storage capacity at ambient temperature, we have created various pore modification strategies. To enhance hydrogen storage in MOFs, we have generated accessible metal sites, fabricated metal nanoparticles or included proper guest molecules in the pores of MOFs, and synthesized MOFs incorporating specific metal binding sites. To selectively capture carbon dioxide from the flue gas or natural gas, which contains not only CO_2 but also other gases, we designed highly flexible MOFs or PCPs with very small pores, which allow CO_2 to open the windows of the materials while prohibiting other gases to enter into the pores. For CO_2 capture at ambient temperature, however, flexibility of the material should be fine-tuned; otherwise it captures CO_2 only at low temperatures. Also, we modified the pores of MOFs by introducing proper guest molecules such as metal ions or polymeric amines, which enhance CO_2 uptake capacity as well as selectivity. Despite that a great deal of efforts has been made in our group and others to develop the materials that can be practically applied in hydrogen storage and carbon dioxide capture, many problems are still left unsolved. Therefore, further studies with innovative ideas should be performed. Perhaps, combination of several strategies presented in this account may lead to development of excellent materials.

7. Acknowledgments

I am very much grateful to the Japan Society of Coordination Chemistry for the International Award 2014, and to the colleagues who were involved in the nomination and selection procedures. I also thank all the past and present members of my laboratory for their contributions and enthusiasm. The research described in this Account was supported by the National Research Foundation of Korea (NRF) Grant funded by the Korean Government (MEST)(no. 2005-0093842).

8. References

1) (a) M. O'Keeffe, O. M. Yaghi, *Chem. Rev.,* **112**, 675 (2012). (b) D. J. Tranchemontagne, J. L. Mendoza-Cortes, M. O'Keeffe, O. M. Yaghi, *Chem. Soc. Rev.*, **38**, 1257 (2009). (c) O. D.-Friedrichs,M. O'Keeffe, O. M. Yaghi, *Phys. Chem. Chem. Phys.,* **9**, 1035 (2007).
2) (a) M. P. Suh, Y. E. Cheon, E. Y. Lee, *Coord. Chem. Rev.*, **252**, 1007 (2008). (b) M. P. Suh, H. R. Moon, *Adv. Inorg. Chem.* **59**, 39 (2007).
3) E. Y. Lee, S. Y. Jang, M. P. Suh, *J. Am. Chem. Soc.*, **127**, 6374 (2005).
4) M. P. Suh, Y. E. Cheon, E. Y. Lee, *Chem. Eur. J.*, **13**, 4208 (2007).
5) M.-H. Choi, H. J. Park, D. H. Hong, M. P. Suh, *Chem. Eur. J.*, **19**, 17432 (2013).
6) H. Kim, M. P. Suh, *Inorg. Chem.*, **44**, 810 (2005).
7) Y. E. Cheon, M. P. Suh, *Chem. Eur. J.*, **14**, 3961(2008).
8) H. J. Choi, M. P. Suh, *J. Am. Chem. Soc.*, **120**, 10622 (1998).
9) M. P. Suh, H. J. Choi, *J. Am. Chem. Soc.*, **124**, 10976 (2002).
10) H. J. Choi, M. P. Suh, *J. Am. Chem. Soc.*, **126**, 15844 (2004).
11) M. P. Suh, H. R. Moon, E. Y. Lee, S. Y. Jang, *J. Am. Chem. Soc.*, **128**, 4710 (2006).
12) H. J. Park, D.-W. Lim, W. S. Yang, T.-R. Oh, M. P. Suh, *Chem. Eur. J.*, **17**, 7251 (2011).
13) H. J. Park, Y. E. Cheon, M. P. Suh, *Chem. Eur. J.*, **16**, 11662 (2010).
14) K. S. Min, M. P. Suh, *J. Am. Chem. Soc.*, **122**, 6834 (2000).
15) H. J. Choi, M. P. Suh, *J. Am. Chem. Soc.*, **126**, 15844 (2004).
16) H. R. Moon, J. H. Kim, M. P. Suh, *Angew. Chem. Int. Ed.*, **44**, 1261 (2005).
17) H. R. Moon, D.-W. Lim, M. P. Suh, *Chem. Soc. Rev.*, **42**, 1807 (2013).
18) Y. E. Cheon, M. P. Suh, *Angew. Chem. Int. Ed.*, **48**, 2899 (2009).
19) (a) H. Furukawa, N. Ko, Y. B. Go, N. Aratani, S. B. Choi, E. Choi, A. O. Yazaydin, R. Q. Snurr, M. O'Keeffe, J. Kim, O. M. Yaghi, *Science*, **239**, 424 (2010). (b) D. Yuan, D. Zhao, D. Sun, H.-C. Zhou, *Angew. Chem. Int. Ed.*, **49**, 5357 **(**2010). (c) O. K. Farha, O. Yazaydın, I. Eryazici, C. Malliakas, B. Hauser, M. G. Kanatzidis, S. T. Nguyen, R. Q. Snurr, and J. T. Hupp, *Nature Chem.*, **2**, 944 **(**2010**).**
20) H. Furukawa, K. E. Cordova, M. O'Keeffe, O. M. Yaghi, *Science*, 341, 1230444 (2013).
21) M. P. Suh, H. J. Park, T. K. Prasad, D.-W. Lim, *Chem. Rev.*, **112**, 782 (2012).
22) (a) O. K. Farha, A. Ö. Yazaydin, I. Eryazici, C. D. Malliakas, B. G. Hauser, M. G. Kanatzidis, S. T. Nguyen, R. Q. Snurr, J. T. Hupp, *Nat. Chem.*, **2**, 944 (2010). (b) H. Furukawa, N. Ko, Y. B. Go, N. Aratani, S. B. Choi, E. Choi, A. Ö. Yazaydin, R. Q. Snurr, M. O' Keeffe, J. Kim, O. M. Yaghi, *Science*, **329**, 424 (2010).
23) T. K. Prasad, D. H. Hong, M. P. Suh, *Chem. Eur. J.*, **16**, 14043 (2010).
24) Y.-G. Lee, H. R. Moon, Y. E. Cheon, M. P. Suh, *Angew. Chem. Int. Ed.*, **47**, 7741 (2008).
25) D.-W. Lim, J. W. Yoon, K. Y. Ryu, M. P. Suh, *Angew. Chem. Int. Ed.*, **51**, 9814 (2012).
26) A. Zaluska, L. Zaluski, J. O. Strom-Olsen, *J. Alloys Compd.,* **288**, 217 (1999)
27) K.-J. Jeon, H. R. Moon, A. M. Ruminski, B. Jiang, C. Kisielowski,

R. Bardhan, J. J. Urban, *Nat. mater.*, **10**, 286 (2011).
28) B. Sakintuna, F. Lamari-Darkrimb, M. Hirscher, *Int J. Hydrogen Energy.*, **32**, 1121 (2007).
29) H. J. Park, M. P. Suh, *Chem. Comm.*, **48**, 3400 (2012).
30) H. J. Park, M. P. Suh, *Chem. Eur. J.*, **14**, 8812 (2008).
31) K. L. Mulfort, O. K. Farha, A. A. Stern, Sarjeant, J. T. Hupp, *J. Am. Chem. Soc.*, **131**, 3866 (2009).
32) K. L. Mulfort, T. M. Wilson, M. R. Wasielewski, J. T. Hupp, *Langmuir*, **25**, 503 (2009).
33) K. L. Mulfort, J. T. Hupp, *Inorg. Chem.*, **47**, 7936 (2008).
34) K. L. Mulfort, J. T. Hupp, *J. Am. Chem. Soc.*, **129**, 9604 (2007).
35) F. Nouar, J. Eckert, J. F. Eubank, P. Forster, M. Eddaoudi, *J. Am. Chem. Soc.*, **131**, 2864 (2009).
36) D.-W. Lim, S. A. Chyun, M. P. Suh, *Angew. Chem. Int. Ed.*, **53**, 7819 (2014).
37) H.-S. Choi, M. P. Suh, *Angew. Chem. Int. Edit.*, **48**, 6865 (2009).
38) T. K. Kim, M. P. Suh, *Chem. Comm.*, **47**, 4258 (2011).
39) D. H. Hong, M. P. Suh, *Chem. Comm.*, **48**, 9168 (2012).
40) H. J. Park, M. P. Suh, *Chem. Sci.*, **4**, 685 (2013).
41) S. Sung, M. P. Suh, *J. Mater. Chem. A*, **2**, 13245 (2014).

Profile

Professor Myunghyun Paik Suh received her B. Sc degree (1971) from Seoul National University in Korea, and M. Sc (1974) and Ph. D. (1976) from The University of Chicago, USA, under the supervision of Professor Virgil L. Goedken. She started her career at Seoul National University on 1977 as an assistant professor, and became an associate professor in 1982. She has been a full professor in 1988-2014. She is currently an emeritus professor at Seoul National University, and also a distinguished chair professor at Hanyang University, Seoul campus. Her research interests focus on chemistry of porous coordination polymers and metal-organic frameworks, and their applications in gas storage, separation, and catalysis. She has received many awards including Korean Science Award, and is a member of The Korean Academy of Science and Technology.